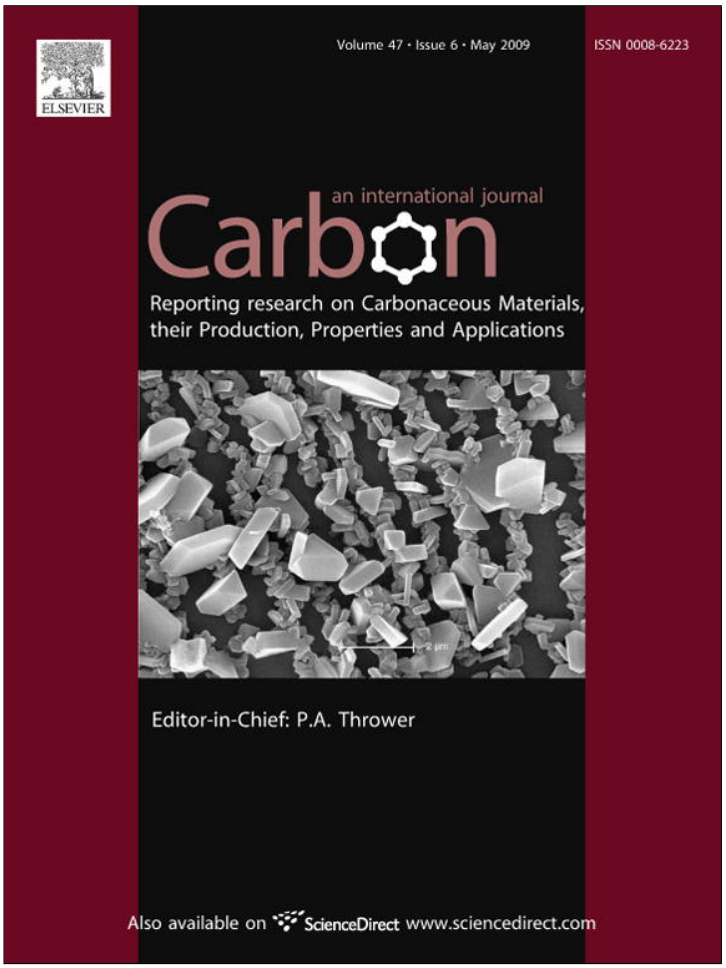

CARBON 47 (2009) 1436–1443

available at www.sciencedirect.com

ScienceDirect

journal homepage: www.elsevier.com/locate/carbon

Enhanced electrochemical and structural properties of carbon cryogels by surface chemistry alteration with boron and nitrogen

Saghar Sepehri[a], *Betzaida Batalla García*[b], *Qifeng Zhang*[a], *Guozhong Cao*[a,*]

[a]*Materials Science and Engineering, University of Washington, 302 Roberts Hall, Box 352120, Seattle, Washington 98195, USA*
[b]*Electronics Characterization Lab, MSE, University of Washington, Mueller 185, Box 352120, Seattle, Washington 98195, USA*

ARTICLE INFO

Article history:
Received 17 July 2008
Accepted 21 January 2009
Available online 31 January 2009

ABSTRACT

Resorcinol–formaldehyde (RF) derived carbon cryogels (CCs) with narrow pore size distribution were obtained via chemical modification using ammonia borane (AB). This chemical modification was achieved by adding AB to the hydrogels during the solvent exchange stage. Nitrogen sorption analysis, scanning electron microscopy (SEM), X-ray photoelectron spectroscopy (XPS), and electrochemical impedance spectroscopy are used to investigate the pore structure, morphology, and electrochemical properties of the modified CCs. After pyrolysis, the AB modified CCs show an increased surface area and larger mesopore volume in comparison to the untreated precursor. In addition, a uniform porous structure with a narrow pore size distribution is produced with a mesopore diameter that does not change significantly during pyrolysis. Moreover, electric double-layer supercapacitors (EDLS) used to characterize the AB modified samples shows pseudocapacitive behavior, higher current density and capacitance.

1. Introduction

Among the porous carbon materials, carbon aerogels (CAs), possessing a range of desirable properties, including tunable mass densities, continuous porosities, and high surface areas, have been the subject of considerable attention for numerous applications [1–6]. The physical, chemical, and electrochemical characteristics of CAs depend strongly on the fabrication method; therefore, different synthesis and processing methods can be used to produce tailored gels for specific applications. CAs can be made from organic hydrogels generated by the sol–gel polycondensation of organic monomers such as resorcinol (R) and formaldehyde (F) in aqueous solution in the presence of a polymerization catalyst [7]. The aerogel is produced by supercritically drying the resorcinol–formaldehyde (RF) hydrogel. Hydrogels may be alternatively subjected to freeze-drying to produce cryogels or be converted into xerogels by vacuum or air drying. Pyrolysis of hydrogels usually decreases the pore volume, pore size and increases microporosity (by IUPAC classification regarding pore widths [8]: micropores <2 nm, mesopores 2–50 nm, and macropores >50 nm) [9]. For many applications, a mesoporous structure with sharp pore size distribution and minimum microporosity is preferred [10]. In addition to tailoring the pore structure, doping carbon gels can provide them with altered or novel properties that expand their applications. An example is that doping carbon with nitrogen and boron has been shown to change the surface chemistry and improve or alter its electrochemical properties [11,12].

In a previous study, we investigated the hydrogen storage properties of a carbon cryogel (CC)–ammonia borane (AB) nanocomposite [13]. It was shown that AB, NH_3BH_3, could be successfully dispersed throughout a CC matrix by soaking CC in AB/THF solution. In this study, we used the same

* Corresponding author: Fax: +1 206 543 3100.
E-mail address: gzcao@u.washington.edu (G. Cao).
0008-6223/$ - see front matter
doi:10.1016/j.carbon.2009.01.034

strategy to produce modified RF hydrogels that are doped with AB, followed by freeze-drying and pyrolysis to generate modified CCs. These materials contain nitrogen and boron, while their porous structure is still maintained. Our investigations confirm that this method homogenously disperses the dopants throughout the CC structure and uniformly changes the CC morphology and structure. The modified CCs in this study, exhibit higher surface area and larger pore volume with a narrow mesopore size distribution. Also, the improvement in the current density and capacitance of the electric double-layer supercapacitors (EDLS) electrodes made from modified carbon cryogels (CCs) indicates the doping elements are active in pseudocapacitive reactions. The nitrogen–boron co-doped mesoporous CCs here reported have the potential to be implemented in a variety of applications, including electrodes for ultracapacitors and batteries in addition to hydrogen storage materials [14–16].

2. Experimental section

2.1. Sample preparation

AB-doped organic cryogels were prepared as previously reported [17]. In general, resorcinol (R) was mixed with formaldehyde (F) solubilized in distilled water (W), using sodium carbonate as a catalyst (C). The R/W ratio was 0.035 g/ml, the R/C ratio was 200:1, and the R/F ratio was 0.5. The clear solutions were then poured into glass vials (inner diameter = 10 mm) that were then sealed and cured at 90 °C for 7 days to complete the gelation process. The precursor dark red and transparent RF hydrogels were placed in ten times their volume of trifluoroacetic acid solution (pH: 1.9) at 45 °C for three days to stop the condensation reaction. Solvent exchange stage, which is necessary for freeze-drying, was carried out by placing the gels in fresh t-butanol ten times their volume at room temperature for 24 h and then repeated twice more with fresh solution. For the modified samples, 2 wt% of AB was dissolved in t-butanol during the first solvent exchange step. The gels, initially dark red in color, changed to light red during this step. The rest of the solvent exchange process was done using fresh t-butanol to avoid the precipitation of residual AB in the pores of the gels. All the samples were freeze dried for a week under vacuum (at −50 °C) to obtain the RF and AB modified (referred hereinafter to as BNRF) cryogels. These cryogels were pyrolyzed for 4 h at 1050 °C (heating rate 5 °C/min and, nitrogen flow 25 ml/min), to produce CCs that are co-doped with boron and nitrogen (referred hereinafter to as BNCC), respectively. Weight loss of the samples during pyrolysis was about 46% for BNCC and 52% for CC sample. The bulk densities of the samples were measured at 0.07 g/cc for CC and 0.09 g/cc for BNCC.

2.2. Nitrogen physisorption, SEM and XPS measurements

The pore structure of CCs was analyzed by means of nitrogen sorption at −196 °C using a Quantachrome NOVA 4200e instrument. The pyrolyzed samples were degassed at a temperature of 300 °C for 24 h. Specific surface area, micropore and mesopore volumes were determined using multi point BET, t-method and BJH analyzes, respectively. Surface morphology of the cross sections of the samples was studied by a JEOL JSM 7000F scanning electron microscope (SEM). RF samples for SEM were Pt coated in order to prevent charging. All X-ray photoelectron spectroscopy (XPS) were done on a thin slice of the samples, using a Surface Science Instruments S-probe spectrometer (sampling depth about 50 Å, X-ray spot size 800 μm).

2.3. Electrochemical measurements

The electrodes were prepared by grinding monoliths into a fine powder then mixed with 3 wt% of polytetrafluoroethylene (PTFE). The resulting electrodes had a thickness of 0.08 mm and a diameter of 9 mm). To test the electrodes a 2-electrode test cell was used with one of the carbon electrodes as the counter and reference electrode. A Celgard® porous film separated the electrodes and to reduce the interfacial effect specially coated aluminum contacts were used. The electrochemical test cell was assembled and sealed under argon. Tetraethylammonium tetrafluoroborate (TEATFB) in saturated 50/50 propylene carbonate/dimethylcarbonate was used as the electrolyte. The equations used to convert the electrochemical data are described elsewhere [18]. The specific quantities in terms of the BET surface area were calculated based on the specific gravimetric quantities of the capacitance and current. The specific capacitance based on the BET surface area was calculated using Eq. (1)

$$C_{BET} = \frac{C_g(F/g)}{SA_{BET}(m^2/g)} \quad (1)$$

where C_g is the gravimetric capacitance of a single electrode and SA_{BET} is the gravimetric specific surface area of the electrode. The current density based on the BET surface area was calculated using Eq. (2)

$$I_{BET} = \frac{I_g(A/g)}{SA_{BET}(m^2/g)} \quad (2)$$

where I_g is the applied current normalized to the mass of the working electrode.

The electrochemical measurements, galvanic cycles (GC), cyclic voltammograms (CV) and electrochemical impedance spectroscopy were performed in a Solartron 1287A using a voltage range between 0 to 2 V. The CV was scanned at 10, 50 and 100 mV/s and the GC measured at 0.5, 1, 5, 10, 50 and 100 mA. Electrochemical impedance spectroscopy was done using the Solartron 1287A in conjunction to the Solartron 1260 FRA/impedance analyzer; the samples were cycled and pretreated at +2 V prior to measurements. An AC voltage amplitude 10 mV and a frequency range of 0.1 MHz–1 mHz was used for the scan.

3. Results and discussion

3.1. Scanning electron microscopy

The SEM images of RF and CC samples are shown in Figs. 1–3. One can see that the modified cryogel samples (BNRF), (Fig. 1b), has a similar morphology to RF samples (Fig. 1a).

However, after pyrolysis CC and BNCC morphology is very different (Figs. 2 and 3). A more ordered porous structure

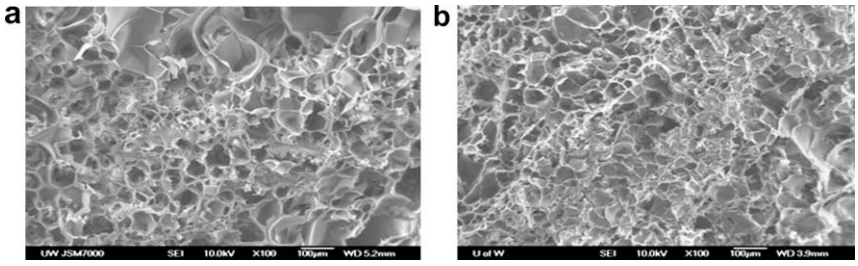

Fig. 1 – SEM images of RF (a) and BNRF (b) samples (scale bar = 100 μm).

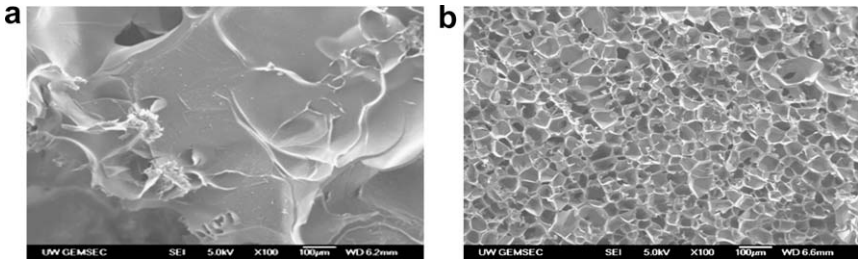

Fig. 2 – SEM images of CC (a) sample and BNCC (b) sample (scale bar = 100 μm).

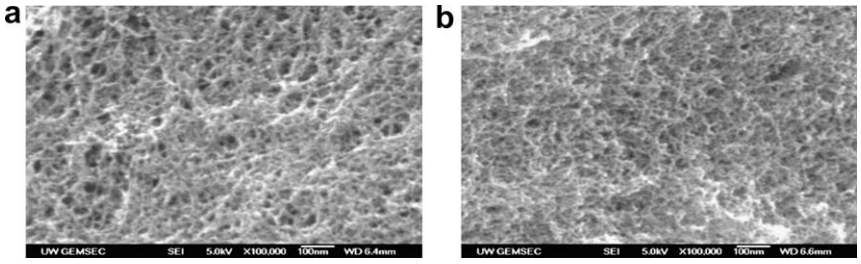

Fig. 3 – SEM images of CC (a) sample and BNCC (b) samples (scale bar = 100 nm).

consisting of smaller particles is observed in the modified sample (Figs. 2 and 3b).

3.2. *X-ray photoelectron spectroscopy (XPS)*

XPS measurements on the cross section of CC samples reveal the elemental changes in the modified sample due to incorporation of AB throughout the carbon structure. Strong C1s, O1s, and B1s peaks were observed in modified sample. In addition, a very weak N1s peak (about 0.1 at%) was observed for the BNCC sample. The relative concentration of each element obtained at two locations of the samples is shown in Table 1. In our study a different surface chemistry is observed for the BNCC sample, where 2.2 wt% boron is observed and oxygen content tripled compared to the CC sample. Also notice the reduction in sodium levels in the BNCC sample. The low N-to-B ratio in the BNCC and the high O content in the BNCC may suggest that the N leaves the pyrolized samples and the B is retained first as B-t-butoxide and then as B-OH after pyrolysis.

Studying the binding energies revealed no significant change for C1s peak in the modified sample. The O1s spectrum shifts from 531 eV in CC sample to 533 eV for the BNCC. The B1s binding energy for BNCC was at 193 eV which is similar to that of B in B_2O_3, while B1s for element B is 187 eV.

3.3. *Nitrogen physisorption*

The nitrogen sorption isotherms for both CC and BNCC samples (Fig. 4) exhibit a type IV isotherm [9], with hysteresis

Table 1 – Elemental distribution at the surface of cryogel samples.

Sample		C	O	Na	B
CC	Atomic content (%)	96.8	2.9	0.3	0
	Mass content (%)	95.6	3.8	0.6	0
BNCC	Atomic content (%)	88.7	8.8	0	2.5
	Mass content (%)	86.4	11.4	0	2.2

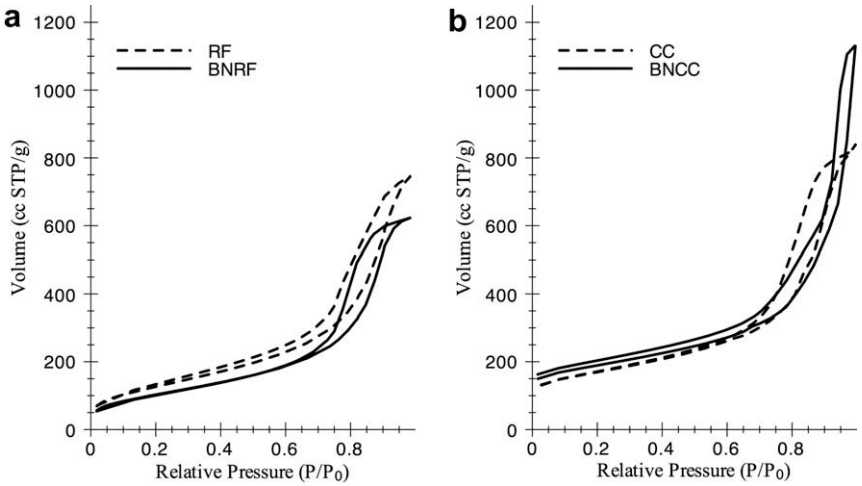

Fig. 4 – Nitrogen sorption isotherms of RF, BNRF (a) and CC, BNCC (b) samples (−196 °C).

associated with the dominance of mesoporosity. Before pyrolysis, the isotherm of the RF sample exhibit larger pore volume and surface area compared to BNRF (Fig. 4a). After pyrolysis the amount of nitrogen adsorbed on CC is only slightly increased from that of its RF precursor. For the BNCC samples, on the other hand, the isotherm shifts toward higher nitrogen adsorption, which suggests an increase in pore volume for BNCC samples compared to BNRF (Fig. 4b).

The pore size distribution of the RF and BNRF samples shows similar distributions with pore radii ca. 5 nm, with the RF sample having a wider distribution (Fig. 5a). After pyrolysis, the pores in the CC sample shift from a 5 nm radius to 16 nm and have a broad distribution of pore sizes. Conversely, in the BNCC sample has a more uniform pore size distribution with a dominant concentration of pores of radius 6 nm appears (Fig. 5b). These structural changes suggest that the boron–nitrogen co-doping alter the carbon structure and prevent changes at least in the mesopore region.

The highly mesoporous structure of the samples is detailed in Table 2. Upon pyrolysis, the specific total surface area, (BET) slightly increases for CC sample. This increase can be attributed to the formation of micropores in the CC sample during the pyrolysis [19]. The modified sample shows a significant increase in the BET surface area after pyrolysis. Micropore volume is small in both samples. The mesopores volume of the CC sample is slightly increased after pyrolysis, while that of BNCC is significantly increased; indicating that the porous network in the BNCC is enhanced by pyrolysis. Also notice that the surface area between the two samples CC and BNCC is not too different from each other. This characteristic will have implications later on in the electrochemical analysis.

3.4. *Electrochemistry*

3.4.1. *Potentiostatic measurements*

Since the capacitance is dependent of the structure of the sample the electrochemical measurements, with the exception of the impedance analysis, are normalized to the total BET surface area for a single electrode. The normalization is possible because the pyrolyzed samples are mostly mesoporous with surface area accessible to charge storage that is >67%. Therefore the formation of the double-layer should not be limited by the micropores [18]. In addition the relation between capacitance and the BET surface area of most of the CC synthesized in our lab (tested under the conditions

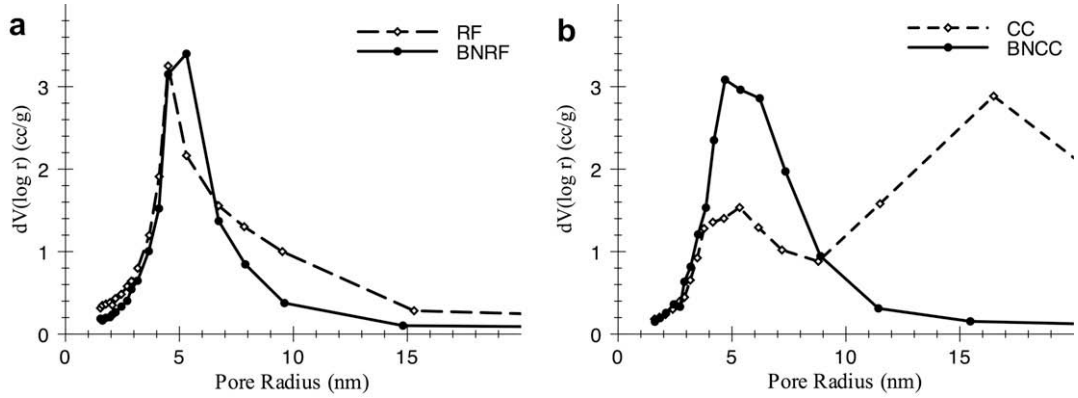

Fig. 5 – Pore size distribution of RF, BNRF (a) and CC, BNCC (b) samples (BJH adsorption).

Table 2 – Porosimetry data for original samples and modified samples before and after pyrolysis.

Sample	BET surface area (m^2/g)	Mesopore surface area (m^2/g %)	Macropore surface area (m^2/g %)	Micropore surface area (m^2/g %)	Mesopore volume (cc/g)	Micropore volume (cc/g)	BJH des. pore radius (nm)
RF	464	359(77)	97(21)	–	1.08	–	4.5
BNRF	377	312(83)	58(15)	–	0.92	–	4.5
CC	567	360(63)	100(18)	106(19)	1.17	0.06	16.0
BNCC	621	316(51)	103(17)	202(33)	1.57	0.11	6.0

described in the experimental section) is linear. The total amount of charge stored per BET surface area of all samples is ca. 0.065 F/m^2. See Fig. 6a and b.

The potentiostatic measurements show a progression of the impact that the nitrogen–boron co-doping has in the carbon substrate. The pseudocapacitive behavior of the BNCC sample is presented in Fig. 7. For the BNCC sample measured at a scan rate of 100 mV/s, two distinct current peaks were observed during the first two cycles (Fig. 7a), but were absent in a similar measurement for the CC sample, Fig. 7b. Such pseudocapacitive behavior may only be attributed to the sample's chemical composition as the aprotic (organic) electrolyte, TEATFB, used does not exhibit pseudocapacitance nor does it decompose in the applied voltage range. Introducing nitrogen or other dopant atoms in carbon structures has been shown to create a pseudocapacitive effect and, thereby, alter their physiochemical properties of double-layer capacitors [20,21]. Although this might be the case more studies are under way since B_2O_3 can affect the surface chemistry as well. The addition of boron compounds like esters can be beneficial for electrode production specially to produce ultrabatteries. Researchers have reported the enhancement of boron modified graphite or other substrates in lead and lithium ultrabatteries [14–16].

Fig. 8 shows the progression for three applied currents. At applied currents of 5 mA and higher, the GC curve is

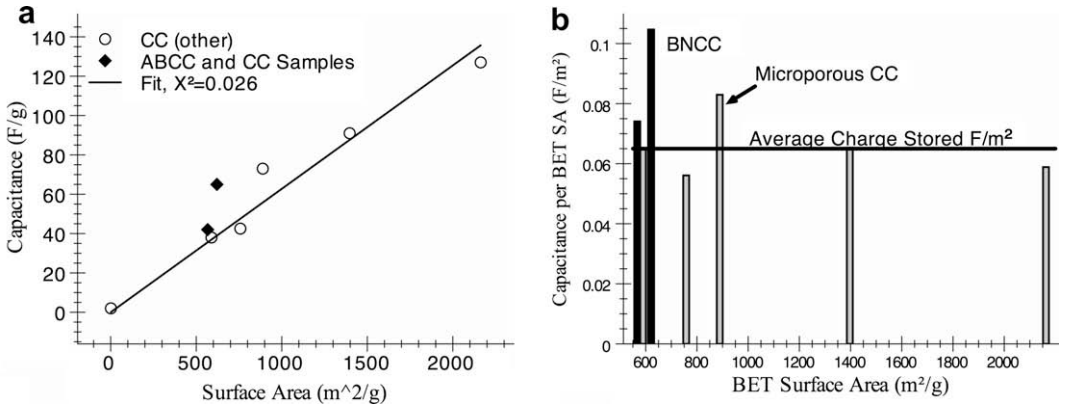

Fig. 6 – (a) Plot of capacitance vs. BET surface area. (b) Charge storage per unit of surface area, BNCC sample has increased charge storage even when considering its low surface area.

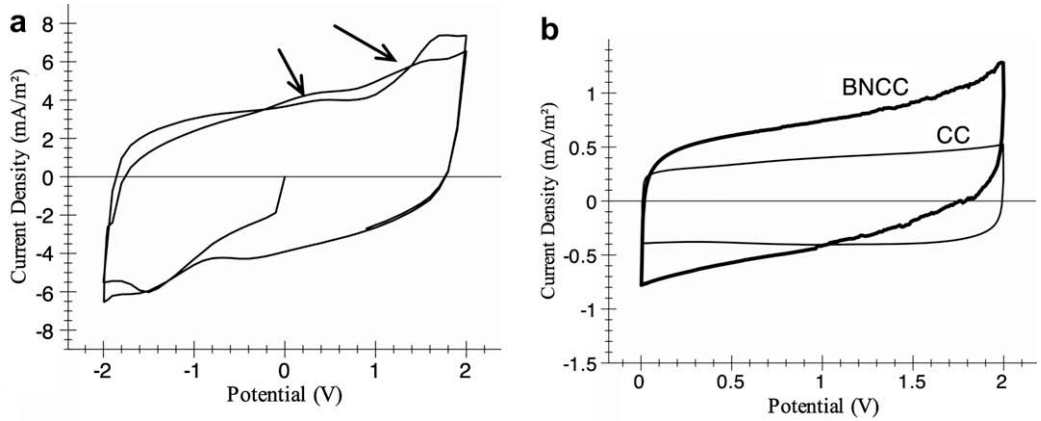

Fig. 7 – (a) First cyclic voltammograms at a rate of 100 mV/s for BNCC, arrows point to faradic reactions. (b) Cyclic voltammogram of AB and CC samples.

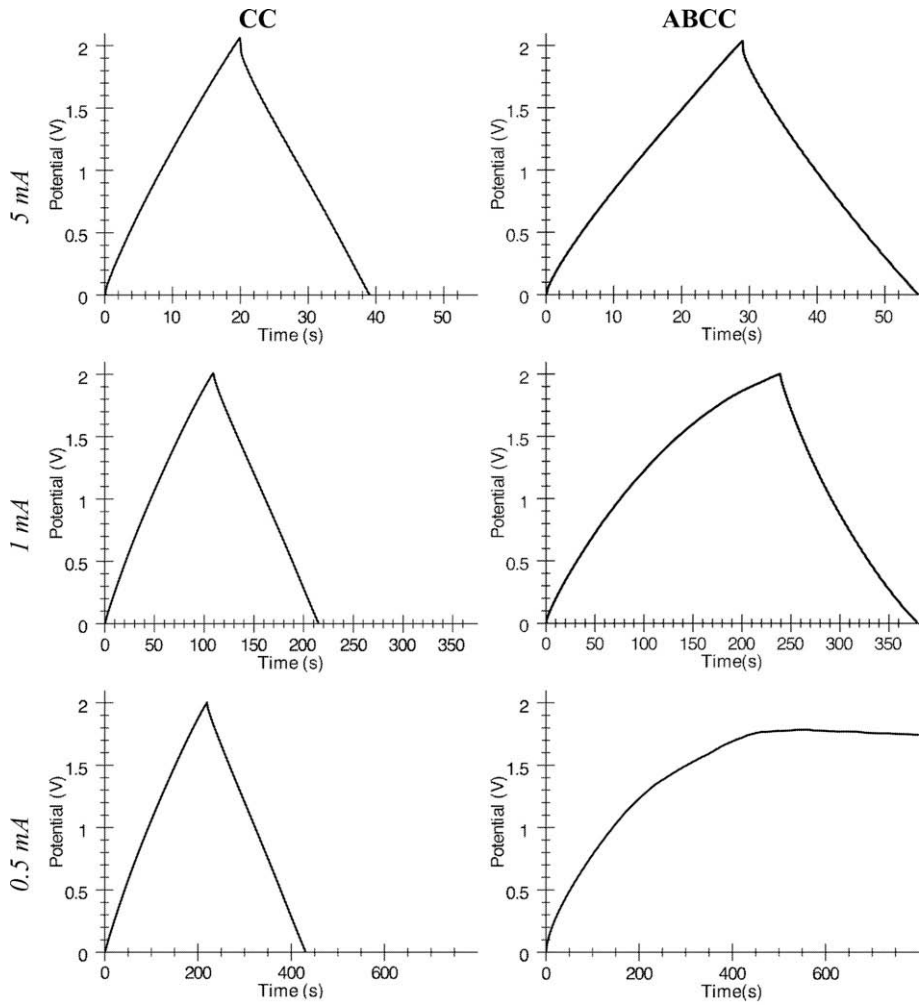

Fig. 8 – Galvanic cycles of CC and ABCC. Notice the ABCC surface modification is chemically active as seen at low currents. The CC sample on the other hand does not exhibit this behavior.

symmetric like that of the CC sample. As the current decreases to 1 mA, the faradic reaction renders the GC curve asymmetric and ultimately at 0.5 mA prevents the capacitor to charge to the intended potential. The asymmetry is evidently due to the reaction involved in the surface modification of the carbon matrix in addition to the new charged species.

After several cycles the samples were tested for overall electrochemical properties to measure the addition of new charged species. The cyclic voltammogram measurements for the BNCC sample had an increased current density over the ones made from CC (Fig. 7b). This increase in current density has been seen in similar systems using boron esters. In addition the capacitance as a function of $1/\sqrt{v}$ for the BNCC device was 30% higher than that of the CC (Fig. 9). This may be the result of two factors: altered pore structure and surface chemistry of the sample. Upon close examination of the surface area and specific capacitance as a function of voltage rate, the pseudocapacitance seems to be the enhancing factor. See Fig. 6a and b. The mesopore surface area of the capacitors is slightly higher in the CC sample than that of the BNCC (460 and 419 m^2/g, respectively) yet the specific capacitance of

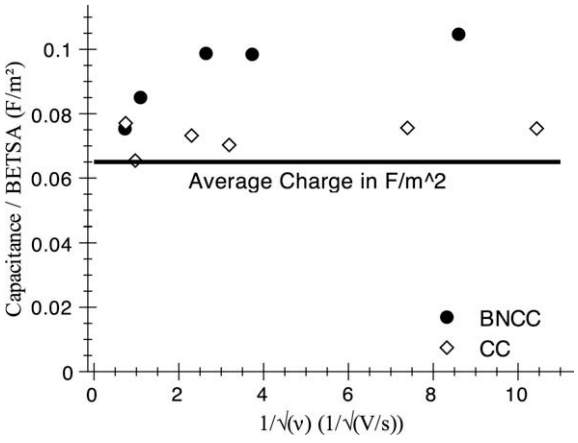

Fig. 9 – Capacitance of samples vs. $1/\sqrt{v}$. The constant behavior of CC is characteristic of mesopores or larger structures that are not affected by the electrolyte penetration [23]. On the other hand pseudocapacitance increases the charge storage capabilities of carbon in the BNCC sample.

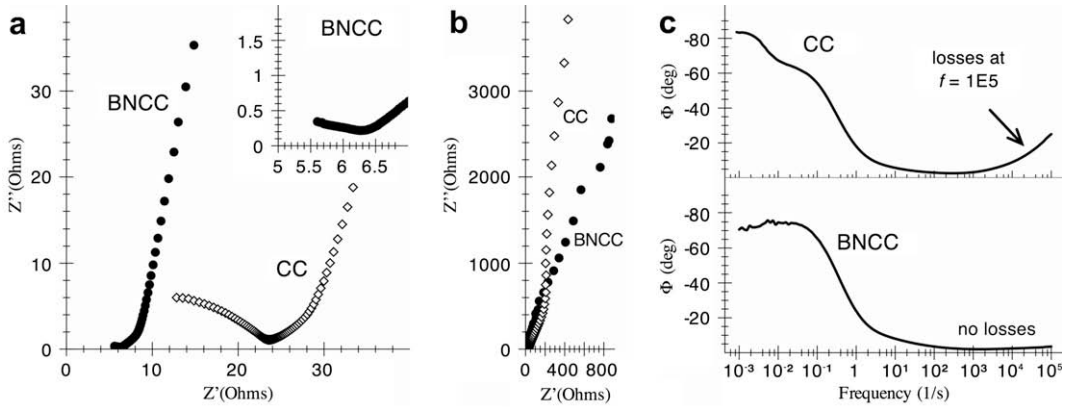

Fig. 10 – (a) Nyquist plot at the high frequency (bulk impedance), (b) low frequency data, (c) phase angle/losses.

the BNCC sample is higher (0.07 and 0.10 F/m^2, respectively). Although it can be argued that micropores are responsible for this increase, a CC sample with much higher surface area of 900 m^2/g (44% higher than BNCC) and mostly micropores can collect a charge of 0.08 F/m^2. It is evident that such increase in the specific capacitance must be faradic in nature mainly dopants or B_2O_3. This improved capacitive behavior has been observed in carbon materials due to the presence of active species that contribute to the total specific capacitance by the pseudocapacitive effect, while large specific surface area and porosity are essential for high current density and charge storage [18,19,21,22].

3.4.2. *Impedance analysis*

Although the potentiostatic measurements can detect the chemical modifications in the BNCC samples, the impedance spectra can separate the role of such modifications. In the BNCC sample the new chemical groups and dopants produce two different responses at the high and low frequency range. (0.1 MHz–1 kHz and < 1 kHz, respectively). In the high frequency range, the Nyquist plot of the two samples (Fig. 10) indicates contrasting effects in their bulk interfacial effect of the electrolyte [18,24]. In double-layer supercapacitors the bulk interfacial effect is due to the relaxation of the electrolyte in large structures like macropores [24]. The CC sample has a wide arch and an ESR of 22 ohms, while the BNCC samples had only a small visible contribution from the bulk interfacial effect at the frequency measured and an ESR of 6.3 ohms. The reduced bulk effect in the BNCC samples is possibly related to the introduction of new charge species since the macropores surface area is nearly the same in both samples as seen in Table 2. The reduction in the ESR is also consistent with the increased current and capacitance as seen in Figs. 7 and 9. After examining the phase angle for high frequency losses, the BNCC sample has nearly no losses at the measured frequency range of 0.1 MHz–1 kHz when compared to the CC sample that has losses that can peak near the 1 MHz region Fig. 10c (This could also account for the missing arch as seen in the insert of Fig. 10a). It is evident from this shift in the high frequency losses that other processes (at frequencies higher than those measured) like relaxations and or ionic processes might be present. I.e. the BNCC chemical modification can reduce the bulk effect by the introduction of new charged species.

However, at the low frequency range, the CC electrodes show signs of pore exhaustion and ideal capacitor behavior [18], while the BNCC samples deviate from ideality also seen in the lower phase angle at $f = 0.01$ (Fig. 10b and c). This deviation is likely due to faradic reactions in the BNCC electrodes (Boron compounds). This observation is also consistent with the asymmetric GC curves of Fig. 8, which increase at low currents. The applied current is proportional to the voltage rate v in electric double-layer capacitors and hence to the frequency of the alternating voltage signal used in the impedance measurements [25]. At low frequencies this faradic reaction produces a resistance consistent with the negative current that prevents the capacitor to charge in Fig. 8.

The electrochemistry results for carbon cryogel samples confirm that the dopant in BNCC samples is electrochemically active and has introduced other charged species during potential cycling, while the CC sample relies completely on the electrolyte for active species in forming the electric double-layers.

4. Conclusions

Nitrogen–boron co-doped CCs (BNCC) can be readily synthesized by homogenous dispersion of AB in RF hydrogel during solvent exchange and followed by freeze-drying and pyrolysis at elevated temperatures in nitrogen, and such co-doping results in significant porous structure change and improved electrochemical properties. Higher mesoporosity, increased pore volume, larger specific surface area, more uniform mesopore size distribution, increased current density and specific capacitance were observed in BNCC samples as compared to CC samples. A further investigation on the effects of separate incorporation of nitrogen and boron in CCs with different pore sizes can be expected to provide additional information for these modified CCs. It is expected these BNCC cryogels can be used to improve the performance of faradic supercapacitors and especially that of batteries.

Acknowledgements

This work has been supported in part by National Science Foundation (DMI-0455994 and DMR-0605159), The University

of Washington Bioenergy IGERT (DGE-0654252) and Air Force Office of Scientific Research (AFOSR-MURI, FA9550-06-1-0326). This work has also been supported by Washington Technology Center, Washington Research Foundation, EnerG2 LLC. XPS measurements were made at the University of Washington NESAC/BIO Surface Analysis Facility.

REFERENCES

[1] Pekala RW, Alviso CT, Kong FM, Hulsey SS. Aerogels derived from multifunctional organic monomers. J Non-Cryst Solids 1992;145(1–3):90–8.
[2] Yamamoto T, Sugimoto T, Suzuki T, Mukai SR, Tamon H. Preparation and characterization of carbon cryogel microspheres. Carbon 2002;40(8):1345–51.
[3] Farmer JLawrence Livermore National Lab c. The use of carbon aerogel electrodes for environmental cleanup. United States: Lawrence Livermore National Lab c; 1996.
[4] Ernest MV, Bibler JP, Whitley RD, Wang NHL. Development of a carousel ion-exchange process for removal of cesium-137 from alkaline nuclear waste. Ind Eng Chem Res 1997;36(7):2775–88.
[5] Petricevic R, Glora M, Fricke J. Planar fibre reinforced carbon aerogels for application in PEM fuel cells. Carbon 2001;39(6):857–67.
[6] Frackowiak E, Beguin F. Carbon materials for the electrochemical storage of energy in capacitors. Carbon 2001;39(6):937–50.
[7] Pekala RW. Organic aerogels from the polycondensation of resorcinol with formaldehyde. J Mater Sci 1989;24(9):3221–7.
[8] Sing KSW, Everett DH, Haul RAW, Moscou L, Pierotti RA, Rouquerol J, et al. Reporting physisorption data for gas solid systems with special reference to the determination of surface area and porosity (recommendations 1984). Pure Appl Chem 1985;57(4):603–19.
[9] Al-Muhtaseb SA, Ritter JA. Preparation and properties of resorcinol–formaldehyde organic and carbon gels. Adv Mater 2003;15(2):101–14.
[10] Ryoo R, Joo SH, Kruk M, Jaroniec M. Ordered mesoporous carbons. Adv Mater 2001;13(9):677–81.
[11] Matsuoka T, Hatori H, Kodama M, Yamashita J, Miyajima N. Capillary condensation of water in the mesopores of nitrogen-enriched carbon aerogels. Carbon 2004;42(11):2346–9.
[12] Frackowiak E. Carbon materials for supercapacitor application. Phys Chem Chem Phys 2007;9(15):1774–85.
[13] Feaver A, Sepehri S, Shamberger P, Stowe A, Autrey T, Cao GZ. Coherent carbon cryogel–ammonia borane nanocomposites for H-2 storage. J Phys Chem B 2007;111(26):7469–72.
[14] Yazd MS, Molazemi A, Moayed MH. The effects of different additives in electrolyte of AGM batteries on self-discharge. J Power Sources 2006;158(1):705–9.
[15] Tabata S, Hirakimoto T, Tokuda H, Susan M, Watanabe M. Effects of novel boric acid esters on ion transport properties of lithium salts in nonaqueous electrolyte solutions and polymer electrolytes. J Phys Chem B 2004;108(50):19518–26.
[16] Bhattacharya A, Basumallick IN. Effect of mixed additives on lead–acid battery electrolyte. J Power Sources 2003;113(2):382–7.
[17] Feaver A, Cao GZ. Activated carbon cryogels for low pressure methane storage. Carbon 2006;44(3):590–3.
[18] Garcia BB, Feaver AM, Zhang Q, Champion RD, Cao GZ, Fister TT, et al. Effect of pore morphology on the electrochemical properties of electric double-layer carbon cryogel supercapacitors. J Appl Phys 2008;104(1):014305–9.
[19] Yamamoto T, Nishimura T, Suzuki T, Tamon H. Control of mesoporosity of carbon gels prepared by sol–gel polycondensation and freeze-drying. J Non-Cryst Solids 2001;288(1–3):46–55.
[20] Kodama M, Yamashita J, Soneda Y, Hatori H, Nishimura S, Kamegawa K. Structural characterization and electric double-layer capacitance of template carbons. Mater Sci Eng B – Solid State Mater Adv Technol 2004;108(1–2):156–61.
[21] Hulicova D, Yamashita J, Soneda Y, Hatori H, Kodama M. Supercapacitors prepared from melamine-based carbon. Chem Mat 2005;17(5):1241–7.
[22] Conway BE. Electrochemical supercapacitors scientific fundamentals and technological applications. NY: Plenum Press; 1999.
[23] Lee JG, Kim JY, Kim SH. Effects of microporosity on the specific capacitance of polyacrylonitrile-based activated carbon fiber. J Power Sources 2006;160(2):1495–500.
[24] Barsoukov E, Macdonald JR. Impedance spectroscopy: theory, experiment, and applications. NJ: Wiley Hoboken; 2005.
[25] Babic B, Kaluderovic B, Vracar L, Krstajic N. Characterization of carbon cryogel synthesized by sol–gel polycondensation and freeze-drying. Carbon 2004;42:2617–24.